processes

MDPI

Article

Impact of Shut-In Time on Acid-Etched Fracture Morphology and Conductivity in SC-CO_2 Acid Fracturing of Tight Dolomite

Chao Liu [1], Jin Lin [1], Yang Gao [1], Qi Hao [1], Jinqiao Wu [1], Wenqi Cao [1], Ke Xu [2,*], Zhan Xie [2] and Bo Gou [2]

[1] Shaanxi Yanchang Petroleum (Group) Co., Ltd., Natural Gas Research Institute Branch, Xi'an 710065, China
[2] State Key Laboratory of Oil and Gas Reservoir Geology and Exploitation, Southwest Petroleum University, Chengdu 610500, China
* Correspondence: axk15928816325@163.com

Abstract

Supercritical CO_2 (SC-CO_2) acid fracturing injects an SC-CO_2-acid mixture into carbonate formations to create high-conductivity channels. It retards acid-rock reaction at high temperature, creating long acid-etched fractures and facilitating CO_2 transport and storage. Fracture conductivity is critical for fluid transport; however, the influence of shut-in time on this property remains poorly understood. In this study, we conducted SC-CO_2 acid-etching experiments and fracture conductivity tests on tight dolomite samples at shut-in times of 0, 30, 60, and 120 min. The interval-averaged acid–rock reaction rates during the 0–30, 30–60, and 60–120 min shut-in periods were 2.23, 3.08, and 2.77 times those during acid injection, respectively. Because temperature increased while residual acid concentration decreased during shut-in, the reaction-rate evolution reflects their combined effects. Fracture morphology exhibited a non-monotonic response to shut-in time. After 30 min, pronounced flow-aligned channels developed along the acid-flow direction, accompanied by a marked increase in surface roughness. At 60 min, channel prominence and roughness amplitude decreased despite continued surface recession, whereas the 120-min fracture exhibited the highest roughness and stronger directional differentiation, with the morphology tending toward flow-perpendicular channels. Fracture conductivity was strongly dependent on closure stress. At 2.5 MPa, conductivity followed the order 30 min > 120 min > 0 min > 60 min, consistent with the ranking of mean and median fracture apertures. In the 25–60 MPa range, the ranking changed to 30 min > 0 min > 120 min > 60 min, indicating the increasing importance of persistent and connected residual flow pathways. Although the 120-min fracture exhibited the highest roughness, its high-stress conductivity remained lower than that of the 30-min fracture, demonstrating that roughness alone is insufficient to determine fracture conductivity. Among the investigated conditions, the 30-min shut-in exhibited the most favorable overall conductivity performance in the 25–60 MPa closure-stress range.

Keywords: shut-in time; SC-CO_2; conductivity; acid etching; carbonate rock

Check for updates

Academic Editor: Liyun Yang

Received: 27 July 2026
Revised: 14 September 2026
Accepted: 15 September 2026
Published: 19 September 2026

Copyright: © 2026 by the authors. Licensee MDPI, Basel, Switzerland. This article is an open access article distributed under the terms and conditions of the Creative Commons Attribution (CC BY) license.

1. Introduction

Carbonate formations are characterized by complex and heterogeneous pore–fracture networks and substantial potential storage space, making them promising targets for geological CO_2 sequestration [1]. However, effectively using this storage capacity depends on establishing highly conductive fluid-transport pathways that enhance CO_2 injectivity and improve connectivity among isolated pore systems, natural fractures, and other storage

domains [2]. Acid fracturing is an important stimulation technique for carbonate reservoirs. During acid fracturing, acid is injected into hydraulic fractures, where differential dissolution of the fracture walls produces non-uniformly etched channels and asperities. These etched features can provide self-support after fracture closure and maintain fluid-flow capacity. Therefore, the morphology of acid-etched fractures and their conductivity under closure stress are important indicators of acid-fracturing performance in carbonate reservoirs [3,4].

Deep carbonate reservoirs commonly exhibit high formation temperatures, in some cases exceeding 100 °C. Elevated temperature substantially accelerates acid–rock reactions, resulting in rapid acid spending near the wellbore and limiting the effective penetration distance of reactive acid, which is unfavorable for generating sufficiently long and conductive acid-etched fractures [5]. To alleviate this limitation, CO_2-energized or CO_2-assisted acid-fracturing technologies have been applied to the stimulation of high-temperature carbonate reservoirs [6]. When the downhole temperature and pressure exceed the critical temperature and pressure of CO_2 (31.1 °C and 7.38 MPa, respectively), CO_2 can exist in the supercritical state [7]. Supercritical CO_2 (SC-CO_2) has low viscosity and a high diffusion coefficient, which facilitate fluid penetration and reduce flow resistance, thereby favoring the development of complex fracture networks [8]. Field applications of CO_2-energized acid fracturing in deep and tight carbonate reservoirs have also demonstrated its potential to reduce the consumption of water-based fluids while improving reservoir stimulation performance [9,10].

A number of experimental studies further indicate that the effect of SC-CO_2 on acid-fracture performance cannot be described as a simple enhancement or deterioration but instead depends on the coupled effects of acid–rock reaction, fracture morphology, and closure stress. Previous studies have shown that blending SC-CO_2 with acid reduces the acid–rock reaction rate with increasing SC-CO_2 content, thereby retarding acid consumption during transport and extending the effective reaction distance; however, this may also produce a flatter etched surface and lower conductivity at moderate closure stresses [11]. Conversely, injecting SC-CO_2 prior to acid can modify the fracture surface and improve the resulting fracture conductivity [12]. More generally, acid system, acid–rock contact time, injection rate, lithology, initial fracture morphology, etching pattern, rock mechanical properties, and closure stress are important factors controlling acid-etched fracture conductivity [13]. Post-injection shut-in has also been incorporated into CO_2-based well-treatment methods to allow the injected treatment fluid to remain in the formation after pumping [14]. Previous studies have also indicated that well shut-in or prolonged post-treatment residence can extend acid–rock interaction after pumping and modify the resulting fracture morphology and conductivity [15–17]. After acid injection is terminated, residual acid retained within the fracture may continue to react with the fracture walls, causing the final etched morphology to evolve further. Acid–rock contact time has been reported to enhance fracture conductivity, although the incremental benefit diminishes after prolonged reaction [17].

Al-Saadoun et al. [18] reported a CO_2-energized acid-fracturing treatment in a deep carbonate gas reservoir in which the well was shut in for 24 h after stimulation. The shut-in period was used to allow the downhole CO_2 temperature to recover toward the in-situ geothermal condition and to provide additional time for acid reaction and diffusion. This field case demonstrates that shut-in has already been recognized as an operational stage in CO_2-energized acid-fracturing treatments. However, only a single shut-in duration was employed, and the effects of systematically varying shut-in time on residual acid reaction, acid-etched fracture morphology, and fracture conductivity were not evaluated.

Although previous studies on SC-CO_2-assisted acid fracturing have investigated the effects of factors such as SC-CO_2 fraction and SC-CO_2–acid injection mode [11,12], previous experimental work has also shown that well shut-in can alter acid-etched fracture morphology and conductivity [16], while field applications have incorporated post-treatment shut-in as an operational stage in CO_2-energized acid-fracturing treatments [18]. However, the effects of systematically varying shut-in duration under SC-CO_2-assisted acid-fracturing conditions remain insufficiently established. In particular, the coupled evolution of residual acid–rock reaction, acid-etched fracture morphology, and stress-dependent conductivity during shut-in remains insufficiently understood. This knowledge gap is important because, unlike the dynamic acid-injection stage, forced fluid flow ceases after shut-in, thereby altering mass-transfer conditions within the fracture. Meanwhile, the residual acid concentration continuously decreases, and the fracture temperature gradually approaches the formation temperature, jointly influencing the subsequent acid–rock reaction and the resulting fracture characteristics. Therefore, whether and how different shut-in durations modify the post-acidizing fracture morphology and conductivity of tight dolomite formations requires further investigation.

To address this knowledge gap, SC-CO_2 acid-etching experiments were conducted on tight dolomite samples at shut-in times of 0, 30, 60, and 120 min. Residual acid concentration measurements, three-dimensional laser scanning, and fracture-conductivity tests were combined to characterize the evolution of acid–rock reaction, acid-etched fracture morphology, and conductivity under increasing closure stress. The areal arithmetic mean height (S_a) and root-mean-square height (S_q) were used to quantify surface-height variations of the etched fractures, while directional profile tortuosity ratios (T_x and T_y), calculated following Lu et al. [19], were used to characterize directional geometric differences in the etched surfaces. By linking reaction, morphology, and conductivity responses across shut-in times, this study clarifies the relationship between shut-in duration and SC-CO_2 acid-fracture performance and identifies a relatively favorable shut-in duration under the investigated experimental conditions. The results provide an experimental basis for understanding shut-in effects in SC-CO_2-assisted acid fracturing and for optimizing shut-in strategies in tight carbonate reservoirs.

2. Experimental Methods

2.1. Materials

Rock samples were collected from Ordovician carbonate outcrops in Linfen City, Shanxi Province, China. All experimental samples were collected from adjacent locations within the same outcrop, and each pair of rock slabs was cut from a single block. X-ray diffraction (XRD) analysis of the four groups of rock powders yielded average mineral compositions as follows: dolomite 94.6%, quartz 1.6%, calcite 3.1%, clay 0.3%, and potassium feldspar plus plagioclase 0.4%. We processed the rock plates into smooth API-standard dimensions (178 mm × 36 mm × 24 mm) to eliminate the influence of initial fracture roughness, and performed X-ray fluorescence (XRF) measurements at six points on each rock slab to further characterize dolomite content, as shown in Figure 1. The results show that the dolomite content across all four groups ranges from 85% to 90%, indicating a relatively uniform mineral distribution on the fracture surfaces and negli-gible interference from other mineral phases (Figure 2). The average permeability of the samples is 0.15 mD. The acid was a field-used gelled acid: 20% HCl + 1.5% corrosion in-hibitor + 0.15% citric acid + 0.5% cleanup additive + 0.55% thickener + 0.5% foaming agent. At a shear rate of 170 s^{-1}, acid viscosity is 14 mPa·s at 90 °C and 7 mPa·s at 120 °C (Figure 3). These acid additives are sourced from Chengdu Lorepthum Technology Co., Ltd., Chengdu, Sichuan Province, China.

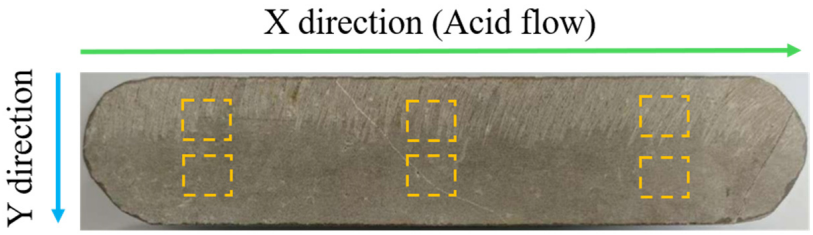


Figure 1. Acid flow direction and sampling locations (The yellow boxes are XRF test points).

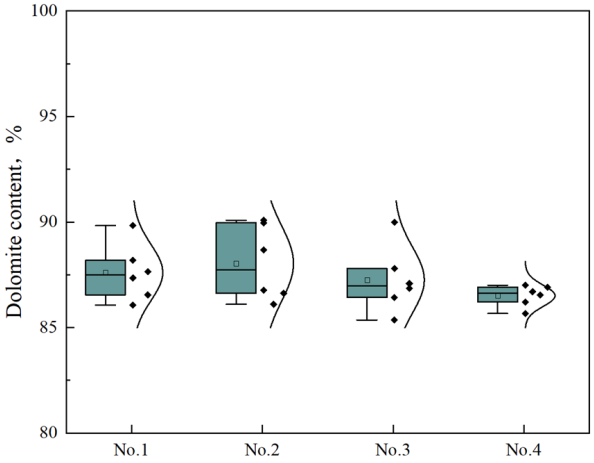


Figure 2. Dolomite content at different sampling locations.

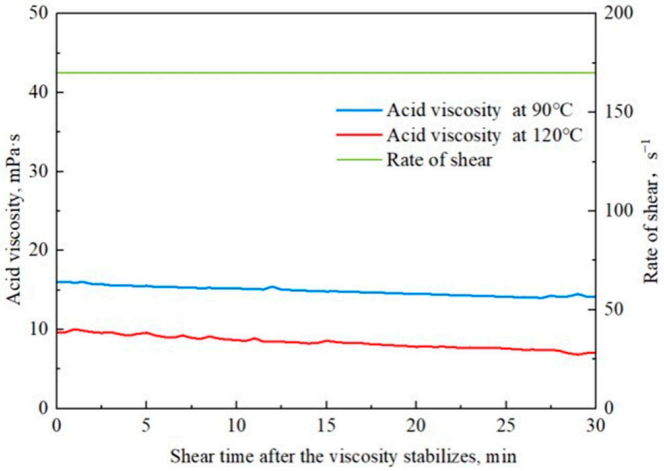


Figure 3. Rheological properties of acid.

2.2. Experimental Device

The experimental setup comprises three core devices: a self-developed SC-CO_2 acid etching device at Southwest Petroleum University, a 3D laser scanning device, and a fracture conductivity testing device (Figure 4). The SC-CO_2 acid etching device converts gaseous CO_2 into SC-CO_2, achieves thorough mixing with acid, and simulates the transport and etching of the mixed fluid in hydraulic fractures. 3D laser scanning device acquires three-dimensional fracture surface data by laser scanning, with a scanning accuracy of up to 0.052 mm. The fracture conductivity testing device applies effective closure stress to the fracture through a hydraulic system and measures conductivity from gas permeability in accordance with Darcy's law, with a maximum load of 2000 kN and a maximum fluid pressure within the fracture of 20 MPa.



(**a**) SC-CO_2 acid etching device (**b**) 3D laser scanning device (**c**) Conductivity testing device

Figure 4. Physical diagram of the key experimental device.

2.3. Experimental Scheme and Procedure

2.3.1. Experimental Scheme

The experimental parameters were designed based on the results of numerical simulations of acid fracturing. In the model, the formation temperature was set to 120 °C, and the field injection rate was 3 m^3/min. Upon completion of the acid-injection stage (120 min), the temperature at the fracture inlet dropped to 84 °C, corresponding to an average temperature of 90 °C during this stage (Figure 5). Therefore, the experimental temperature during the acid-injection stage was set to 90 °C. The primary objective of this study is to investigate the effect of shut-in on fracture morphology and conductivity in SC-CO_2 acid-etching. Because the slab-simulated fracture is small-scale and to ensure safe, stable laboratory operation, the acid-injection duration was reduced to 30 min. The laboratory injection rate was determined using the Reynolds-number similarity criterion for power-law fluid flow in fractures [20]. The Reynolds numbers for acid-fluid flow at engineering scale and at laboratory scale are shown in Equation (1) and Equation (2), respectively. Equation (3) can be obtained by equating the two, and the displacement at the experimental scale can be calculated. The scaling procedure accounts for differences in fracture geometry and the non-Newtonian rheological behavior of the acid system, resulting in a laboratory injection rate of 200 mL/min. The parameters used for the scaling calculation are summarized in Table 1. Applying the same 30-min acid-injection stage to all specimens provided consistent pre-shut-in acid-rock interaction conditions, allowing the effects of shut-in duration to be compared under the same injection protocol. As shown in Table 2, four shut-in conditions of 0, 30, 60, and 120 min were investigated. One independent fracture specimen, consisting of a matched pair of rock slabs cut from the same rock block, was tested for each shut-in condition.

$$N_{\mathrm{Re,f}} = \frac{\rho q_{\mathrm{f}}^{2-n} w_{\mathrm{f}}^{2n-2}}{2 \times 3^{n-1} k h_{\mathrm{f}}^{2-n} \left(\frac{2n+1}{3n}\right)^{n-1}} \tag{1}$$

$$N_{\mathrm{Re,1}} = \frac{\rho q_{1}^{2-n} w_{1}^{2n-2}}{6^{n-1} k h_{1}^{2-n} \left(\frac{2n+1}{3n}\right)^{n-1}} \tag{2}$$

$$q_{1} = \frac{q_{\mathrm{f}} h_{1}}{2 h_{\mathrm{f}}} \left(\frac{w_{\mathrm{f}}}{w_{1}}\right)^{\frac{2n-2}{2-n}} \tag{3}$$

where $N_{\mathrm{Re,f}}$ and $N_{\mathrm{Re,l}}$ are Reynolds numbers for acid-fluid flow at engineering scale and at laboratory scale, respectively, dimensionless; ρ is density of acid solution, kg/m^3; q_{f} is injection rate at engineering scale, m^3/s; w_{f} is field fracture width, m; k is Power-law coefficient, Pa·s^n; h_{f} is field fracture height, m; n is power-law flow-behavior index for the acid, dimensionless, and is obtained from rheological experiments; q_{l} is experimental

injection rate, m^3/s; w_l is experimental fracture width, m; h_l is experimental plate width, m. The value of n used in the present scaling calculation was 0.146, obtained by fitting the rheological data of the acid system to the power-law model.

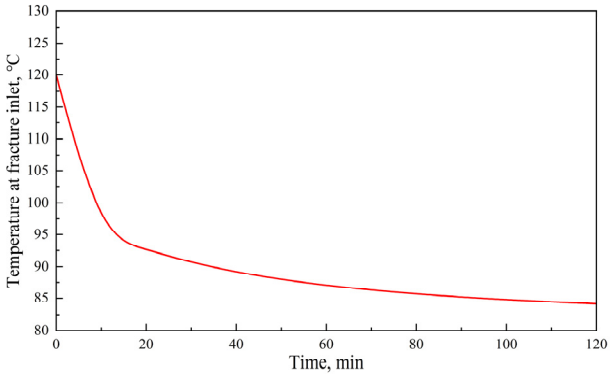


Figure 5. Temperature change characteristics at the fracture entrance during the acid treatment stage.

Table 1. Experimental displacement calculation data.

q_f (m^3/min)	h_f (m)	w_f (m)	n	h_l (m)	w_l (m)	q_l (mL/min)
3	90	0.0066	0.146	0.036	0.002	200

Table 2. Experimental scheme.

No.	Acid Injection Stage			Shut-In Well Stage		
	Temperature °C	Pumping Rate mL/min	Time min	Temperature °C	Pumping Rate mL/min	Time min
1	90	200	30	/	0	0
2				90–110		30
3				90–115		60
4				90–118		120

2.3.2. Experimental Procedure

The experimental procedure is illustrated in Figure 6 and described as follows:

(1) Rock plates were dried, and fracture surface elevation data were obtained via a 3D laser scanning device. The acid concentration was measured after preparation.

(2) The rock slabs were placed in the slab holder of the supercritical carbon dioxide acid-etching apparatus. After the temperature was raised to 90 °C, the SC-CO_2–acid mixture was injected for 30 min. Subsequently, the injection of the mixture was stopped, the holder was sealed, and the temperature of the core holder heating system was set to the formation temperature of 120 °C to simulate heat conduction from the reservoir to the fracture and the fluids within it. The acid-etching experiment during the shut-in stage was then carried out, and internal temperature sensors recorded real-time temperature data throughout the process.

(3) Acid-etched rock plates were removed and dried, and 3D laser scanning was performed again to obtain three-dimensional data of the fracture surfaces. After cropping the interpolated data outside the fracture surface, the elevation data of the fracture surface were plotted as cloud maps to quantitatively characterize the roughness and morphological features of the fracture surface, so as to reveal the effects of shut-in time on fracture morphology.

(4) Fracture conductivity was measured using a conductivity testing apparatus with nitrogen as the test gas. Considering the relatively high closure stress applied during the test,

the closure stress was increased stepwise in increments of 2.5 MPa to minimize the risk of rock-plate damage caused by rapid loading and to ensure controlled stress application. The closure stress was progressively increased to the reservoir closure stress of 60 MPa. At each target closure-stress level, the applied stress was maintained for 30 min to allow the pressure response of the fracture system to stabilize before conductivity measurements were recorded. Fracture conductivity was then determined at three prescribed nitrogen flow rates selected within the test range of 50–300 mL/min. For each flow condition, the gas flow rate and pressure differential across the fracture were monitored and used to calculate the corresponding fracture conductivity. Three conductivity values were therefore obtained at each closure-stress level under different gas-flow conditions, and their arithmetic mean was reported as the representative fracture conductivity at that stress level. The same procedure was repeated as the closure stress was increased in 2.5-MPa increments until 60 MPa was reached.

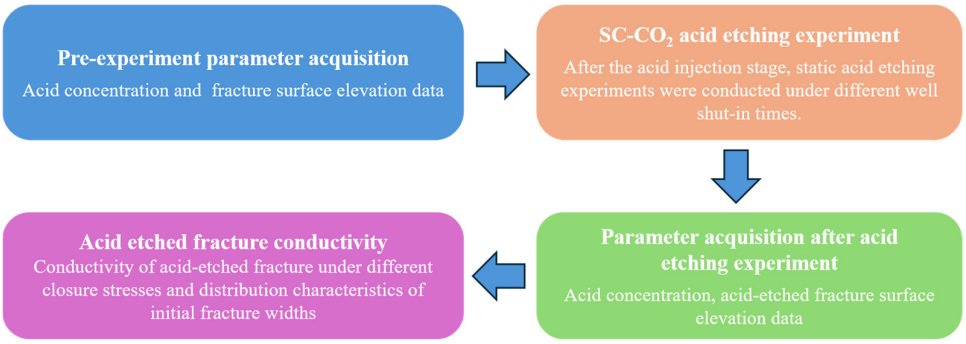


Figure 6. Experimental testing procedure.

3. Results and Discussion

3.1. Acid-Rock Reaction Rate Under Various Shut-In Times

Acid–rock reaction rate is an important parameter characterizing the acid-etching performance. In this study, the acid concentration was measured after each experimental run, and the concentration difference between two consecutive runs was determined. The average reaction rates for different shut-in stages were then calculated using Equation (4). For example, the average reaction rate during the shut-in period of 0–30 min can be obtained from the data of Experiments No. 1 and No. 2. The residual acid concentration of the post-reaction solution was determined using a consistent analytical procedure. The collected acid samples were diluted at a fixed ratio before pH measurement, and the concentrations of Ca^{2+} and Mg^{2+} were subsequently determined after neutralization with $NaHCO_3$. To reduce measurement variability, the same sampling volume, dilution ratio, neutralization procedure, instrument calibration procedure, and analytical conditions were maintained throughout all tests.

$$d = \frac{(C_{i-1} - C_i)\rho_{acid}}{100 M_{HCl} \Delta t_i} \quad (4)$$

where d is the interval-averaged acid–rock reaction rate, mol/(mL·s); C_{i-1} is the acid concentration after the reaction in the previous stage, wt%; C_i is the post-etching average acid concentration, wt%; ρ_{acid} is the acid density, g/mL; M_{HCl} is the molecular weight of HCl, g/mol; Δt_i is the duration of the corresponding reaction interval, s.

As shown in Figure 7, after the reaction in the previous stage during the 120-min shut-in period, temperature increases logarithmically, while the average acid concentration decreases nearly linearly. During the acid injection stage at 90 °C, the average acid concentration is 19.3%, and the acid-rock reaction rate is 2.18×10^{-7} mol/(mL·s). During

the 0–30 min shut-in period, temperature increased from 90 °C to 110 °C, with an average acid concentration of 17.8%, and the reaction rate was 2.23 times that during acid injection. During the 30–60 min period, the temperature increased from 110 to 115 °C, the average acid concentration decreased to 14.3%, and the reaction rate reached its maximum value, 3.08 times that during acid injection. During the 60–120 min period, the temperature increased further from 115 to 118 °C, the average acid concentration decreased to 10.5%, and the reaction rate decreased to 2.77 times that during acid injection.

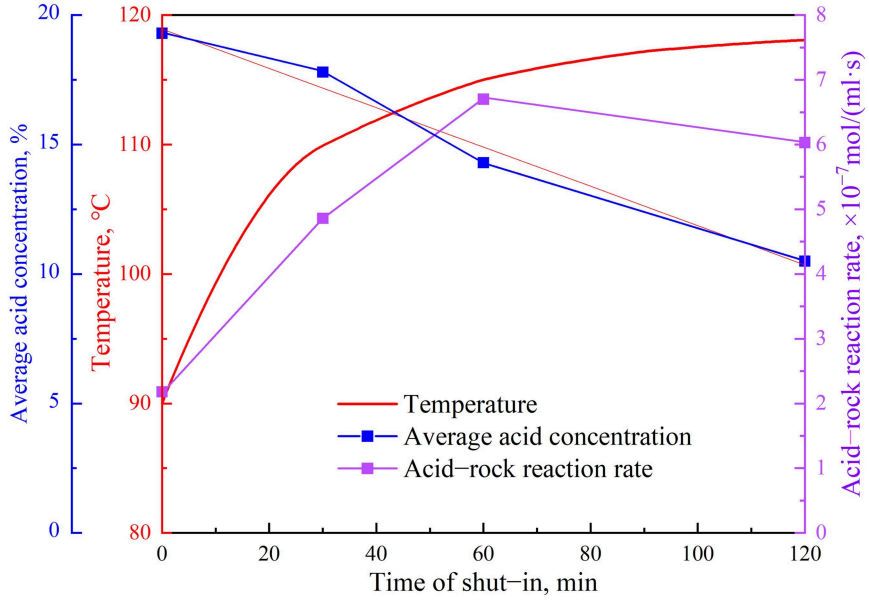


Figure 7. Acid-rock reaction rates at different well shut-in times.

During shut-in, temperature increased continuously, while average acid concentration decreased due to ongoing acid consumption. The evolution of reaction rate therefore reflected the combined influence of the changing thermal environment and acid availability. Overall, the average acid–rock reaction rate during shut-in is substantially higher than that during acid injection, implying that extended acid–rock contact in the shut-in period influences fracture surface morphology evolution. Moreover, the reaction rates observed across different shut-in intervals indicate that the 60–120 min period may exert a weaker effect on acid dissolution compared with the 0–60 min period.

3.2. Acid-Etched Fracture Morphology

Acid-etched fracture morphology is an important indicator of the acid-etching performance and plays an important role in determining fracture conductivity [13,21]. Three-dimensional laser-scanning data were used to construct elevation maps of the acid-etched fracture surfaces for qualitative characterization of surface morphology. The fracture surfaces were scanned with a spatial sampling interval of 0.1 mm. The areal arithmetic mean height (S_a) and root-mean-square height (S_q) were calculated from the surface-height data to quantitatively characterize the amplitude of surface-height variations. In addition, directional profile tortuosity ratios were calculated along the X- and Y-directions following the method of Lu et al. [19]. For each direction, the actual length of each surface profile was calculated by summing the distances between adjacent scanning points and was normalized by its projected length. The directional tortuosity ratios T_x and T_y were then obtained by averaging the tortuosity ratios of all profiles along the X- and Y-directions, respectively. Thus, all profiles within the effective scanned area were included in the calculation. For consistency, the X direction was defined as parallel to the acid-flow direction and is hereafter referred to as the flow-aligned direction, whereas the Y direction was defined as

perpendicular to the acid-flow direction and is referred to as the flow-perpendicular direction. Larger values of T_x and T_y indicate greater geometric tortuosity in the flow-aligned and flow-perpendicular directions, respectively. The directional tortuosity difference was defined as ΔT. Thus, a positive ΔT indicates greater tortuosity in the flow-perpendicular direction, whereas a negative ΔT indicates greater tortuosity in the flow-aligned direction. Accordingly, channels extending preferentially along the X direction are referred to as flow-aligned channels, whereas those extending preferentially along the Y direction are referred to as flow-perpendicular channels.

The areal arithmetic mean height (S_a) and root-mean-square height (S_q) were calculated as:

$$S_a = \frac{1}{MN}\sum_{i=1}^{M}\sum_{j=1}^{N}\left|z_{ij} - \bar{z}\right| \tag{5}$$

$$S_q = \sqrt{\frac{1}{MN}\sum_{i=1}^{M}\sum_{j=1}^{N}\left(z_{ij} - \bar{z}\right)^2} \tag{6}$$

where M and N are the numbers of sampling points in the X- and Y-directions, respectively, and z_{ij} is the surface height at point (i,j) relative to the mean plane.

The directional tortuosity ratios in the X- and Y-directions were calculated as:

$$T_x = \frac{1}{N}\sum_{j=1}^{N}\frac{\sum_{i=1}^{M-1}\sqrt{(\Delta x)^2 + \left(z_{i+1,j} - z_{i,j}\right)^2}}{(M-1)\Delta x} \tag{7}$$

$$T_y = \frac{1}{M}\sum_{i=1}^{M}\frac{\sum_{j=1}^{N-1}\sqrt{(\Delta y)^2 + \left(z_{i,j+1} - z_{i,j}\right)^2}}{(N-1)\Delta y} \tag{8}$$

where Δx and Δy are the sampling intervals in the X- and Y-directions, respectively. The difference in directional tortuosity was defined as:

$$\Delta T = T_y - T_x \tag{9}$$

where a larger T_x or T_y indicates greater profile tortuosity in the corresponding direction.

As shown in Figures 8 and 9, the fracture surface before acid etching was relatively smooth, with a mean surface elevation of approximately 24.00 mm. At 0 min shut-in (No. 1), the etched surface remained relatively flat, with only minor local protrusions near the edges and natural fracture regions and no obvious dissolution pits. The mean surface elevation decreased slightly to 23.57 mm. Correspondingly, S_a and S_q were only 0.07018 and 0.09428 mm, respectively, while T_x and T_y were 1.00306 and 1.00174, indicating limited surface relief and geometric tortuosity.

After 30 min of shut-in (No. 2), pronounced flow-aligned channels developed preferentially along the acid-flow (X) direction, accompanied by numerous dissolution pits, and elongated etched features. Although the mean surface elevation decreased only slightly from 23.57 to 23.51 mm, S_a and S_q increased markedly to 0.21574 and 0.26258 mm, respectively, indicating that pronounced surface heterogeneity developed before substantial overall surface recession occurred. Meanwhile, T_x and T_y increased to 1.00823 and 1.00925, respectively. The slightly higher T_y indicates greater geometric variation along the Y-direction profiles. Because these profiles intersect the preferential grooves extending along the X direction, this directional relationship is consistent with the development of

flow-aligned (X-oriented) channels. Nevertheless, the small difference between T_x and T_y indicates that the overall directional anisotropy remained relatively weak at this stage.

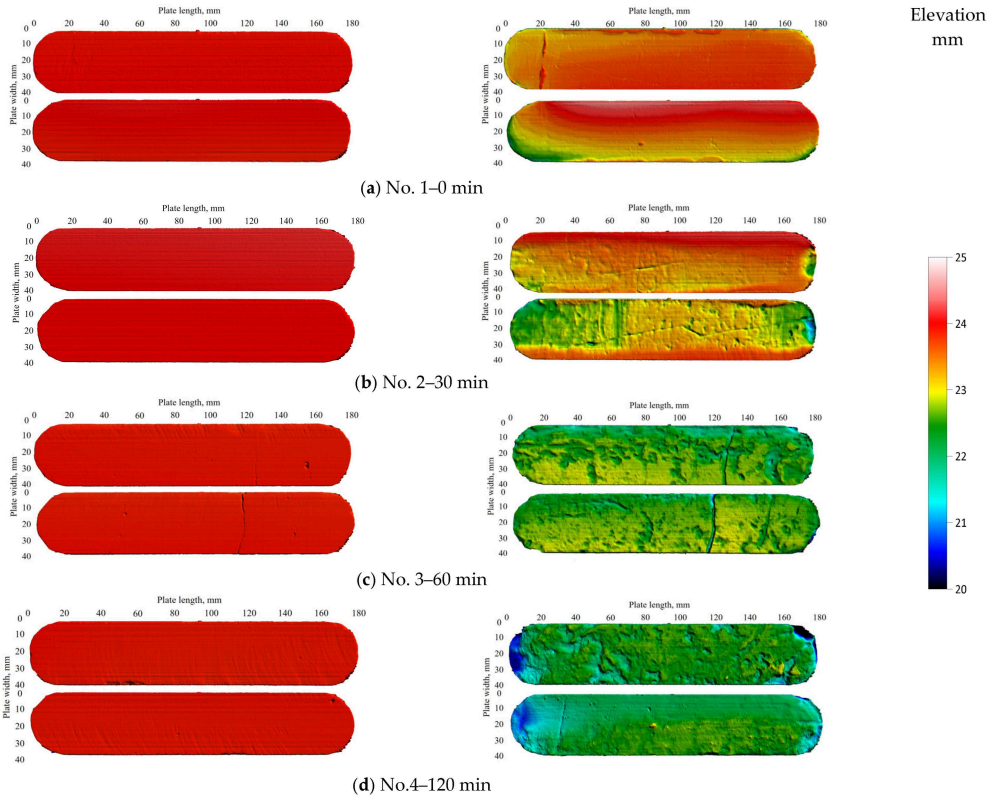


Figure 8. Elevation maps of acid-etched fracture surfaces under various shut-in times (left and right are before and after acid-etching, respectively).

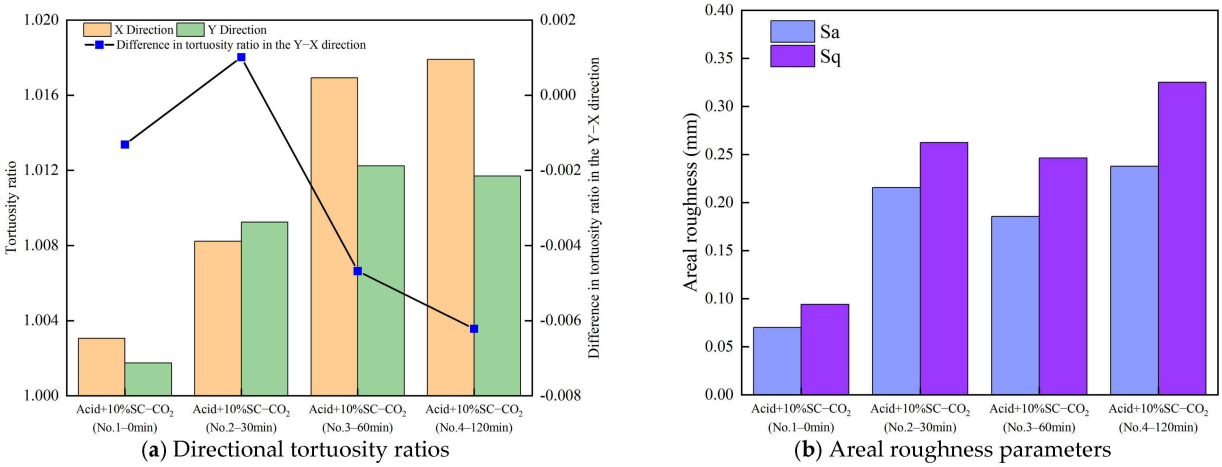


Figure 9. Quantitative morphological parameters of acid-etched fracture surfaces under different shut-in times.

At 60 min of shut-in (No. 3), the mean surface elevation decreased markedly to 22.48 mm, indicating substantially greater material removal. In contrast, S_a and S_q decreased to 0.18547 and 0.24647 mm, respectively. This change is consistent with the elevation map, in which dissolution became more broadly distributed over the fracture surface rather than remaining concentrated within the previously developed channels, thereby reducing the overall height contrast. Meanwhile, T_x and T_y further increased to 1.01692 and 1.01224, respectively, and ΔT changed from 0.00102 to −0.00468. The sign reversal in ΔT indicates a change in the directional characteristics of the etched morphology. Specifically,

$T_x > T_y$ indicates stronger geometric variation along the X-direction profiles, suggesting that the preferential etched features increasingly tended to extend along the Y direction, corresponding to a transition from the predominantly flow-aligned morphology observed at 30 min toward a more flow-perpendicular morphology.

After 120 min of shut-in (No. 4), the mean surface elevation further decreased to 21.00 mm, while large and tortuous acid-etched channels became dominant and isolated dissolution pits became less prominent. Both roughness parameters reached their maximum values, with S_a = 0.23775 mm and S_q = 0.32519 mm, reflecting the pronounced surface relief produced by these large-scale etched features. T_x increased further to 1.01791, while T_y decreased slightly to 1.01170, resulting in the largest directional difference ($\Delta T = -0.00621$). The larger magnitude of the negative ΔT indicates that the directional anisotropy became more pronounced during prolonged shut-in. In conjunction with the surface morphology, the higher T_x relative to T_y suggests a stronger tendency for the dominant etched channels to extend along the Y direction, corresponding to a predominantly flow-perpendicular channel morphology.

In summary, surface modification during the acid-injection stage was relatively limited, whereas shut-in substantially altered the etched morphology and promoted the development of heterogeneous, channelized fracture surfaces. At 30 min of shut-in, S_a and S_q increased markedly despite only a small decrease in mean surface elevation, indicating that pronounced surface relief developed with relatively limited material removal. The slightly higher T_y than T_x is consistent with the preferential development of flow-aligned channels along the X direction, while the small difference between T_x and T_y indicates that the overall directional anisotropy remained relatively weak. With further shut-in to 60 and 120 min, material removal became more extensive, and the increasing difference between T_x and T_y indicated progressively stronger directional anisotropy. In particular, the reversal from $T_y > T_x$ at 30 min to $T_x > T_y$ at longer shut-in times suggests a shift in the dominant orientation of the etched features from the flow-aligned X direction toward the flow-perpendicular Y direction.

3.3. Effect of Shut-In Time on Conductivity

To quantitatively characterize the fracture aperture, the mean aperture w, median aperture w_{50}, and coefficient of variation CV_w were calculated as:

$$w = \frac{1}{N}\sum_{i=1}^{N} w_i \tag{10}$$

$$w_{50} = \text{median}(w_i) \tag{11}$$

$$CV_w = \frac{s_w}{\overline{w}} \times 100\% \tag{12}$$

where w_i is the local fracture aperture, N is the number of measurement points, and s_w is the standard deviation of the aperture distribution. The mean and median apertures characterize the overall and representative fracture openings, respectively, whereas CV_w reflects spatial heterogeneity in the fracture aperture. The calculated results are summarized in Table 3.

Figure 10 presents the variation in fracture conductivity with closure stress; Figure 11 presents the distribution of fracture aperture under different shut-in times. At 2.5 MPa, the conductivity follows the order No. 2 (30 min) > No. 4 (120 min) > No. 1 (0 min) > No. 3 (60 min), consistent with the ranking of the mean and median fracture apertures summarized in Table 3. In particular, No. 2 exhibits the largest mean and median apertures of 2.80 and 2.70 mm, respectively, with a moderate CV_w of 29%, whereas No. 3 has the smallest corresponding apertures of 0.82 and 0.73 mm and the highest CV_w of 36%. This quantitative

correspondence indicates that available fracture opening is the dominant geometrical control on conductivity under low closure stress, consistent with findings from conventional studies on acid-etched fracture conductivity [13]. The higher heterogeneity and smaller representative aperture of No. 3 also suggest poorer continuity of effective flow pathways.

Table 3. Statistical parameters of fracture aperture at different shut-in times.

Fracture	Shut-In Time (min)	Mean Aperture w (mm)	Median Aperture w_{50} (mm)	CV_w (%)
No. 1	0	1.39	1.33	24
No. 2	30	2.80	2.70	29
No. 3	60	0.82	0.73	36
No. 4	120	2.04	1.91	33

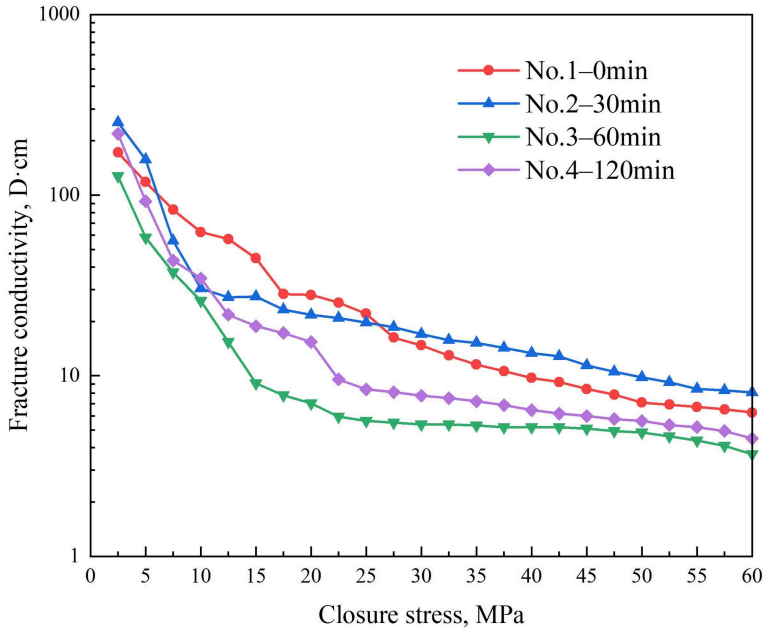


Figure 10. Conductivity of SC-CO_2 acid-etched fractures under various shut-in times.

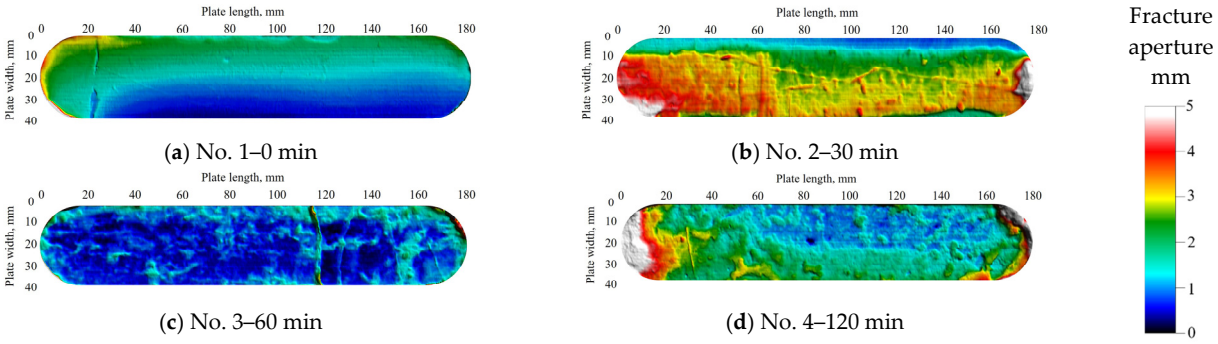


Figure 11. Distribution of fracture aperture under different shut-in times.

As closure stress increases, the conductivity of No. 2, No. 3, and No. 4 decreases more rapidly than that of No. 1. The transition from rapid to slower conductivity decline occurs at approximately 10, 12.5, 15, and 17.5 MPa for No. 2, No. 4, No. 3, and No. 1, respectively. This difference reflects the combined influence of fracture aperture and acid-etched morphology on the closure response. Pronounced surface relief and locally narrow regions promote preferential asperity contact and deformation during initial loading, whereas the relatively weak relief of No. 1 leads to more gradual closure. Therefore, a rapid

initial conductivity reduction does not necessarily indicate poor conductivity retention at elevated closure stress.

The conductivity ranking changes to No. 1 > No. 2 > No. 4 > No. 3 at approximately 12.5–15 MPa and subsequently to No. 2 > No. 1 > No. 4 > No. 3 above 25 MPa. This evolution indicates that the dominant control shifts from fracture opening at low closure stress toward the persistence and connectivity of residual flow pathways at higher closure stress. Notably, No. 4 exhibits the highest roughness (S_a = 0.23775 mm and S_q = 0.32519 mm), but its conductivity above 25 MPa remains lower than that of No. 2, demonstrating that roughness amplitude alone cannot determine fracture conductivity. Instead, conductivity is governed by the combined effects of fracture aperture, aperture heterogeneity, surface relief, directional morphology, and residual-channel connectivity.

Among the four tested conditions, the 30-min shut-in fracture provides the most favorable combination of large fracture opening, developed surface relief, limited directional differentiation, and persistent residual flow pathways. Consequently, No. 2 maintains the highest conductivity above 25 MPa despite its relatively rapid initial decline. Therefore, 30 min is identified as the most favorable shut-in duration under the present experimental conditions.

3.4. Research Limitations and Future Perspectives

This study experimentally investigated the influence of shut-in duration on the evolution of acid–rock reactions, acid-etched fracture morphology, and conductivity in SC- CO_2-assisted acid fracturing. Under a fixed acid-injection time of 30 min, a favorable shut-in duration was identified within the range of 0–120 min. It should be noted that, owing to the inherent heterogeneity of natural carbonate rocks, only a limited number of specimens with similar and uniformly distributed mineral compositions could be obtained, which constrained the implementation of systematic replicate experiments. However, because this work focuses on shut-in duration as the only variable, mineralogical differences among the rock samples were minimized to highlight the effect of shut-in time. In addition, the laboratory specimen dimensions, acid-treatment scale, and maximum shut-in duration are considerably smaller than field conditions; thus, the trends under longer shut-in periods and reservoir-scale conditions require validation through numerical simulations and pilot tests. Meanwhile, carbonate rocks are typically characterized by anisotropy, which can significantly affect acid-etching behavior [21,22], and the reaction properties involving SC- CO_2 are known to be strongly influenced by temperature and pressure [23–25]. The present study, however, did not reveal the changes in various physicochemical properties of SC-CO_2 during shut-in. Therefore, future research should explore the roles of mineral composition, distribution, and SC-CO_2 properties such as permeability, heat-transfer performance, and wettability during the acid-etching process to elucidate the underlying mechanisms.

Overall, the present results provide experimental support for the optimization of shut-in strategies, while extending the shut-in period and conducting multi-field coupled simulations remain key priorities for future research.

4. Conclusions

In this study, SC-CO_2 acid etching experiments and fracture conductivity tests under different shut-in times to investigate their effects on acid–rock reaction behavior, fracture morphology, and conductivity. The following conclusions are drawn:

(1) The interval-averaged acid–rock reaction rates during the 0–30, 30–60, and 60–120 min shut-in periods were 2.23, 3.08, and 2.77 times those during the acid-injection stage, respectively. Because temperature increased while residual acid concentration decreased during shut-in, the observed reaction-rate evolution reflects the combined changes in thermal conditions and acid availability.

(2) Shut-in time induced a non-monotonic evolution of the acid-etched fracture morphology. Without shut-in, the fracture surface remained relatively uniform. After 30 min of shut-in, pronounced flow-aligned channels developed preferentially along the acid-flow direction, accompanied by a marked increase in surface roughness. At 60 min of shut-in, these channels became less prominent despite continued surface recession. After 120 min, the fracture surface exhibited greater roughness and stronger directional differentiation, with the dominant etched features gradually shifting from the flow-aligned direction toward the flow-perpendicular direction.

(3) Fracture conductivity was strongly dependent on closure stress. At 2.5 MPa, conductivity followed the order 30 min > 120 min > 0 min > 60 min, consistent with the ranking of the mean and median fracture apertures, indicating that fracture opening is the dominant geometrical control under low closure stress. In the 25–60 MPa closure-stress range, the conductivity ranking shifted to 30 min > 0 min > 120 min > 60 min, indicating that the persistence and connectivity of residual flow pathways become increasingly important as the fracture closes. Although the 120-min fracture exhibited the highest surface roughness, its conductivity remained lower than that of the 30-min fracture under high closure stress, demonstrating that surface roughness alone is insufficient to determine fracture conductivity. Among the investigated conditions, the 30-min shut-in exhibited the most favorable overall conductivity performance in the 25–60 MPa closure-stress range.

These results clarify the relationship between shut-in-induced fracture morphology and conductivity and provide experimental support for optimizing SC-CO_2 acid fracturing in tight carbonate formations. However, because only one independent fracture specimen was tested for each shut-in condition, inter-sample variability was not quantified. Further replicate experiments and scale-up studies are therefore needed to evaluate the reproducibility and broader applicability of the observed trends.

Author Contributions: Conceptualization, C.L. and K.X.; Methodology, C.L., J.L. and K.X.; Validation, J.L., Y.G., Q.H. and J.W.; Formal analysis, C.L. and W.C.; Investigation, C.L.; Resources, Y.G.; Data curation, C.L. and W.C.; Writing—original draft, C.L.; Writing—review & editing, C.L., J.L., K.X. and B.G.; Visualization, Z.X.; Supervision, J.W. and K.X.; Project administration, Y.G. and Q.H.; Funding acquisition, J.L. and J.W. All authors have read and agreed to the published version of the manuscript.

Funding: This research was funded by the Shaanxi Provincial Key Research and Development Program (No. 2025CY-YBXM-612). Their support is gratefully acknowledged.

Data Availability Statement: Data will be made available on request.

Conflicts of Interest: Authors Chao Liu, Jin Lin, Yang Gao, Qi Hao, Jinqiao Wu, and Wenqi Cao were employed by Shaanxi Yanchang Petroleum (Group) Co., Ltd. The remaining authors declare that the research was conducted in the absence of any commercial or financial relationships that could be construed as a potential conflict of interest.

References

1. Zhao, J.; Zhang, Z.; Xiao, Y.; Hou, S.; Li, P.; Zhang, S. Controlling Mechanisms of CO_2 Sequestration Efficiency in Tight Carbonate Gas Reservoirs: Experimental Insights into Pore-Throat Constraints and Mineralogical Responses. *RSC Adv.* **2025**, *15*, 22556–22564. [CrossRef] [PubMed]
2. Orivri, U.D.; Chanda, P.; Johnson, L.; Koehn, L.W.; Pollyea, R.M. Opportunities and Challenges for Geologic CO_2 Sequestration in Carbonate Reservoirs: A Review. *Int. J. Greenh. Gas Control* **2025**, *142*, 104342. [CrossRef]
3. Li, N.; Dai, J.; Liu, P.; Luo, Z.; Zhao, L. Experimental Study on Influencing Factors of Acid-Fracturing Effect for Carbonate Reservoirs. *Petroleum* **2015**, *1*, 146–153. [CrossRef]
4. Zhang, R.; Hou, B.; Zhou, B.; Liu, Y.; Xiao, Y.; Zhang, K. Effect of Acid Fracturing on Carbonate Formation in Southwest China Based on Experimental Investigations. *J. Nat. Gas Sci. Eng.* **2020**, *73*, 103057. [CrossRef]

5. Li, Y.; Jiang, X.; Tang, J.; Liu, B. Simulation Study of Acid Fracturing Initiation with Consideration of Rock Mechanics Parameter Variations. *Rock Mech. Rock Eng.* **2024**, *57*, 5743–5761. [CrossRef]
6. Abdullah, A.; Al-Othman, M.; Al-Enezi, A.; Shtail, M.; Ateyah, M.; Al-Mousharji, M.; Bhatia, K.; Alboueshi, A.; Abdelbaky, A.; Eid, W. First CO_2 Energized-Fracturing Technology in Highly Depleted and Tight Reservoir Unlocks Vast Potential: Case Study from North Kuwait Field. In Proceedings of the ADIPEC, Abu Dhabi, United Arab Emirates, 31 October–3 November 2022.
7. Sanchez, M.; Abel, J.T.; Idris, M.; Soriano, E.; Lopez, A.; Fathkutdinov, D. Acid Fracturing Tight Gas Carbonates Reservoirs Using CO_2 to Assist Stimulation Fluids: An Alternative to Less Water Consumption While Maintaining Productivity. In Proceedings of the SPE Middle East Unconventional Resources Conference and Exhibition, Muscat, Oman, 26–28 January 2015.
8. Wu, L.; Hou, Z.; Luo, Z.; Xiong, Y.; Zhang, N.; Luo, J.; Fang, Y.; Chen, Q.; Wu, X. Numerical Simulations of Supercritical Carbon Dioxide Fracturing: A Review. *J. Rock Mech. Geotech. Eng.* **2023**, *15*, 1895–1910. [CrossRef]
9. Malik, A.R.; Dashash, A.A.; Driweesh, S.M.; Noaman, Y.M.; Soriano, E.; Lopez, A. Successful Implementation of CO_2 Energized Acid Fracturing Treatment in Deep, Tight and Sour Carbonate Gas Reservoir in Saudi Arabia That Reduced Fresh Water Consumption and Enhanced Well Performance. In Proceedings of the SPE Middle East Oil & Gas Show and Conference, Manama, Bahrain, 8–11 March 2015.
10. Liu, P.; Barakat, A.K.; Kalabayev, R.; Salem, A.M.; Pochetnyy, V.; AlOthman, F.; Almatroud, N.; Baidas, A.W.; Al-Othman, M.R.; Samad, Z.M.A. Combination of CO_2 Foam and Fit-For-Purpose Fluids During Acid Fracturing Revive Potential of a Jurassic Well in a Depleted, High-Temperature Carbonate Reservoir in North Kuwait. In Proceedings of the ADIPEC, Abu Dhabi, United Arab Emirates, 31 October–3 November 2022.
11. Gou, B.; Li, X.; Guo, J.; Liu, C.; Chen, C.; Guan, C. Experimental Investigation of the Impacts of Supercritical Carbon Dioxide on Acid-Etching Fracture Morphology and Conductivity in Tight Carbonate Reservoir. *Fuel* **2024**, *360*, 130526. [CrossRef]
12. Gou, B.; Xu, K.; Wang, X.; Li, X.; Guo, J. Effect of SC-CO_2–Acid Injection Mode on Fracture Morphology and Conductivity of CO_2-Energized Acid-Fracturing in Tight Carbonate Rocks: An Experimental Study. *Pet. Sci.* 2026, *in press*. [CrossRef]
13. Liu, P.; Hu, H.; Chen, X.; Du, J.; Liu, J.; Liu, F.; Chen, W.; Jia, Y. The Influencing Parameters and Improve Methods of Acid-Etched Fracture Conductivity: A Review. *Geoenergy Sci. Eng.* **2024**, *238*, 212844. [CrossRef]
14. Decker, R.L.; Hyman, M.D.; Ridge, J.J. CO_2 Foamed Well Treatments. U.S. Patent No. 7,464,754 B1, 16 December 2008.
15. Bilden, D.M.; Fletcher, P.A.; Montgomery, C.T.; Guillory, R.J.; Allen, T.P. The Effect of Long-Term Shut-in Periods on Fracture Conductivity. In Proceedings of the SPE Annual Technical Conference and Exhibition, Dallas, TX, USA, 22–25 October 1995.
16. Liu, C.; Gou, B.; Guan, C.; Guo, J.; Li, X.; Wang, X.; Wei, D.; Hao, S.; Shen, F.; Wang, N. Effect of Well Shut-in on Acid Etching Morphology and Conductivity. *J. China Univ. Pet.* **2021**, *45*, 96–103.
17. Jia, H.; Pu, H.; Li, J.; Wang, J.; Chen, X.; Mou, J.; Gao, B. Acid-Etched Fracture Conductivity with In Situ-Generated Acid in Ultra-Deep, High-Temperature Carbonate Reservoirs. *Processes* **2024**, *12*, 1792. [CrossRef]
18. Al-Saadoun, D.; Al-Mefleh, K.; Al-Saeed, A.; Ajayi, A.; Ghaempanah, B.; Fidan, E.; Barki, J. Restoration of Long Term Closed in, New Jurassic Gas Well, Long-Time Shut-In Due to a Sinking Wellhead Followed by the Rigless Activation Using CO_2 Energized Acid Hydrofrac and Successful Realization of Production. In Proceedings of the Kuwait Oil & Gas Show, Kuwait City, Kuwait, 3–5 February 2026.
19. Lu, C.; Bai, X.; Luo, Y.; Guo, J. New Study of Etching Patterns of Acid-Fracture Surfaces and Relevant Conductivity. *J. Pet. Sci. Eng.* **2017**, *159*, 135–147. [CrossRef]
20. Chen, C.; Tan, X.; Guo, J.; Zeng, J.; Zhang, H.; Liu, K.; Wang, S. Experimental Study on Acid Etching and Rough Fracture Conductivity of Carbonate Rocks Using Digital Carving Technology. *Processes* **2026**, *14*, 545. [CrossRef]
21. Mou, J.; Xia, X.; Gao, B.; Zhang, S.; Ma, X.; Wang, F. Effect of Mixed Mineralogy on Etching Profile and Conductivity in Acid Fracturing in Naturally Fractured Carbonate Reservoirs. In Proceedings of the Paper presented at the International Petroleum Technology Conference, Dhahran, Saudi Arabia, 12–14 February 2024.
22. Yang, J.; Min, J.; Peng, J.; Li, Q.; Wang, Z. Anisotropy of Surface Morphology of Carbonate Rocks after Reaction with Acid. *J. Pet. Explor. Prod. Technol.* **2024**, *14*, 2853–2869. [CrossRef]
23. Wu, J.; Li, Q.; Li, Q.; Wang, F.; Cheng, Y.; Yan, C. Design and Optimization of Bottom-Hole Temperature–Pressure Combinations in Gas Production from Gas Hydrates via Carbon Dioxide Replacement Strategy. *Energies* **2026**, *19*, 3536. [CrossRef]
24. Rangel-Jurado, N.; Kong, X.; Kottsova, A.; Morales, L.; Ma, N.; Games, F.; Brehme, M.; Bernasconi, S.; Saa, M. Reactivity of Wet SC-CO_2 toward Reservoir and Caprock Formations under Elevated Pressure and Temperature Conditions: Implications for CCS and CO_2-Based Geothermal Energy Extraction. *Energy Fuels* **2025**, *39*, 1679–1693. [CrossRef] [PubMed]
25. An, Q.; Zhang, Q.; Li, X.; Yu, H.; Zhang, X. Experimental study of temperature and pressure effects on rock damage caused by SC-CO_2. *Geothermics* **2023**, *114*, 102797. [CrossRef]

Disclaimer/Publisher's Note: The statements, opinions and data contained in all publications are solely those of the individual author(s) and contributor(s) and not of MDPI and/or the editor(s). MDPI and/or the editor(s) disclaim responsibility for any injury to people or property resulting from any ideas, methods, instructions or products referred to in the content.